



CHORUS

This is the accepted manuscript made available via CHORUS. The article has been published as:

Ground-State Phase Diagram of a Spin-Orbital-Angular-Momentum Coupled Bose-Einstein Condensate

Dongfang Zhang, Tianyou Gao, Peng Zou, Lingran Kong, Ruizong Li, Xing Shen, Xiao-Long Chen, Shi-Guo Peng, Mingsheng Zhan, Han Pu, and Kaijun Jiang

Phys. Rev. Lett. **122**, 110402 — Published 20 March 2019

DOI: [10.1103/PhysRevLett.122.110402](https://doi.org/10.1103/PhysRevLett.122.110402)

Ground-state phase diagram of a spin-orbital-angular-momentum coupled Bose-Einstein condensate

Dongfang Zhang¹, Tianyou Gao¹, Peng Zou², Lingran Kong^{1,6}, Ruizong Li^{1,6}, Xing Shen^{1,6},
Xiao-Long Chen⁴, Shi-Guo Peng^{1,*}, Mingsheng Zhan^{1,5}, Han Pu^{3,5}, and Kaijun Jiang^{1,5†}

¹*State Key Laboratory of Magnetic Resonance and Atomic and Molecular Physics,
Wuhan Institute of Physics and Mathematics, Chinese Academy of Sciences, Wuhan, 430071, China*

²*College of Physics, Qingdao University, Qingdao 266071, China*

³*Department of Physics and Astronomy, and Rice Center for Quantum Materials, Rice University, Houston, Texas 77251, USA*

⁴*Centre for Quantum and Optical Science, Swinburne University of Technology, Melbourne 3122, Australia*

⁵*Center for Cold Atom Physics, Chinese Academy of Sciences, Wuhan, 430071, China and*

⁶*School of Physics, University of Chinese Academy of Sciences, Beijing 100049, China*

(Dated: December 28, 2018)

By inducing a Raman transition using a pair of Gaussian and Laguerre-Gaussian laser beams, we realize a ⁸⁷Rb condensate whose orbital angular momentum (OAM) and its internal spin states are coupled. By varying the detuning and the coupling strength of the Raman transition, we experimentally map out the ground-state phase diagram of the system for the first time. The transitions between different phases feature discontinuous jump of the OAM and the spin polarization, and hence are of first-order. We demonstrate the hysteresis loop associated with such first-order phase transitions. The role of inter-atomic interaction is also elucidated. Our work paves the way to explore exotic quantum phases in the spin-orbital-angular-momentum coupled quantum gases.

Coupling between particle's spin and orbital motion is ubiquitous in optics [1], atomic physics and condensed-matter physics [2, 3]. Ultracold atoms with high tunability provide an ideal platform to study the spin-orbit coupling. Spin-linear-momentum (SLM) coupling in quantum gases is achieved by inducing Raman transition in the atom with two counter-propagating laser fields [4–6], in which the linear momentum of the light field can be transferred to the atom. SLM coupling possesses spatial translational symmetry and has a continuous spectrum. A variety of exotic quantum states have been observed in quantum gases with SLM coupling [4–12]. Photons can also carry orbital angular momentum (OAM). For example, Laguerre-Gaussian (LG) optical field contains a phase factor $e^{il\phi}$, where ϕ is the azimuthal angle and the integer l is the winding number of the optical vortex [13], and carries an OAM of $l\hbar$. What happens to atoms if they encounter light carrying OAM is an intriguing question. Recently several theoretical works proposed another fundamental type of spin-orbit coupling, namely the spin-orbital-angular-momentum (SOAM) coupling, and predicted rich quantum phases in atomic Bose condensate [14–19]. The SOAM coupling preserves the rotational symmetry and possesses a discrete spectrum. Thus atomic condensates subjected to SOAM and to SLM exhibit distinct properties.

SOAM coupling is achieved by inducing atomic Raman transition with a pair of co-propagating laser fields that carries different OAMs, as schematically illustrated in Fig. 1 (a). The relative winding phase of the photons is transferred to the atoms during the Raman transition. Using this method, SOAM has been demonstrated in both dynamically expanding [20, 21] and trapped atomic condensates [22, 23]. However, up until now, a system-

atic experimental investigation of the ground-state phase diagram of the system is still lacking.

Our current work reports the first experimental observation of the ground-state phase diagram and the associated phase transition in an SOAM coupled condensate. Across the phase boundaries, the vorticity of the atomic wave function and the spin polarization exhibit discontinuous jumps, providing clear evidence that the associated phase transition is of first-order. We further demonstrate the hysteresis loop that represents another hallmark of a general first-order phase transition. Under the situation where the single-particle ground state is two-fold degenerate, we show that all the atoms condense into one of the degenerate states. This can be attributed to the effect of many-body interaction: if both states are populated, the system has to pay an energy penalty due to the additional quantum exchange interaction.

In the experiment, we produce a ⁸⁷Rb condensate, with an atom number of $1.2(1) \times 10^5$, in a nearly spherical optical dipole trap with trapping frequency $\omega = 2\pi \times 77.5$ Hz, as in our previous work [24]. As shown in Fig. 1 (a) and (b), a pair of Raman beams ($l_1 = -2$ and $l_2 = 0$) copropagate along the z direction, suppressing the SLM coupling. The absolute winding number difference $|\Delta l|$ of the two Raman beams equals to 2. Compared to the case of $|\Delta l| = 1$ [20–23], a larger winding number difference enriches the phase diagram in our scheme [14, 16]. Choosing a combination of a Gaussian and an LG optical fields also makes it easy to align the Raman beams with BEC and reach the threshold optical power of the phase transition (see Supplemental Material [25]). The relative winding phase of the two light fields is transferred to the condensate in the Raman transition process between two atomic spin states $|\uparrow\rangle = |F = 1, m_F = 0\rangle$ and

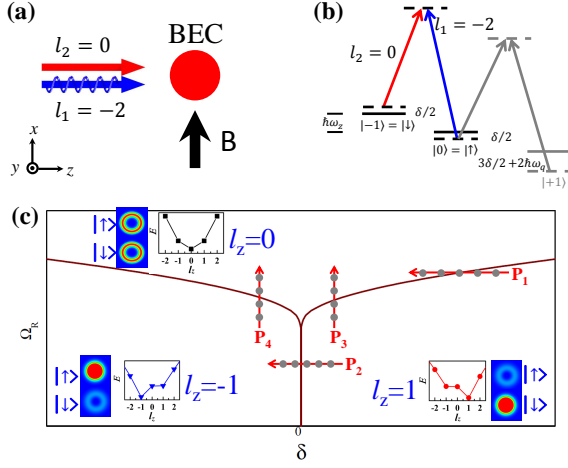


FIG. 1. (color online) Scheme of the SOAM coupling. (a) Experimental schematics. Two laser beams with different OAM ($l_1 = -2$ and $l_2 = 0$) copropagate along the z -axis and interact with the Rb condensate. The magnetic field is along the x -axis. (b) Energy level diagram. Two $\lambda = 790.02$ nm lasers couple two spin states $|\uparrow\rangle = |F = 1, m_F = 0\rangle$ and $|\downarrow\rangle = |F = 1, m_F = -1\rangle$. δ is the two-photon detuning of the Raman transition. $\omega_q = 2\pi \times 5.52$ kHz is the quadratic Zeeman shift. (c) The single-particle phase diagram. Three quantum phases are denoted by the quasi-orbital-angular momentum $l_z = 1, 0, -1$, respectively. $P_{1,2,3,4}$ represent four different paths that cross phase boundaries. The representative dispersion curve and the spin-dependent atomic density distribution for each phase are also shown.

$|\downarrow\rangle = |F = 1, m_F = -1\rangle$. A bias magnetic field produces a large quadratic Zeeman shift $\omega_q = 2\pi \times 5.52$ kHz, which makes the spin state $|F = 1, m_F = +1\rangle$ off resonant and negligible. We use the tune-out wavelength $\lambda = 790.02$ nm of the two Raman beams [26], in which the ground spin manifold of the Rb atom experiences no scalar AC stark shift. This can make sure that any vortex structure observed in the condensate is produced due to the SOAM coupling, not the trapping effect of the LG beam [20]. We probe the spin-resolved spatial distribution of the atoms with the aid of a gradient magnetic field using time-of-flight (TOF) imaging with 20 ms expansion time.

Our system can be described by an effective single-particle Hamiltonian (see Supplemental Material [25])

$$\hat{H}_0 = \hat{H}_{ho} + \frac{\delta}{2}\hat{\sigma}_z + \Omega(\rho)\hat{\sigma}_x - \frac{l\hbar}{M\rho^2}\hat{L}_z\hat{\sigma}_z + \frac{(l\hbar)^2}{2M\rho^2}, \quad (1)$$

where $l = (l_1 - l_2)/2$, $\hat{\sigma}_{x,z}$ are Pauli matrices, $\hat{H}_{ho} \equiv (-\hbar^2/2M)\nabla^2 + M\omega^2\rho^2/2$ with $\mathbf{r} = (\rho, \phi, z)$, $\hat{L}_z = -i\hbar\partial_\phi$ denotes the quasi-orbital-angular-momentum operator of atoms along the z -axis, δ is the two-photon detuning, $\Omega(\rho) = \Omega_R(\rho/w)^{|l_1|+|l_2|}e^{-2\rho^2/w^2}$ represents the spatial dependent Raman coupling characterized by the coupling strength Ω_R , and w is the waist of the two Raman beams. Here $-(l\hbar/M\rho^2)\hat{L}_z\hat{\sigma}_z$ is the SOAM coupling term. \hat{H}_0

clearly conserves the quasi-angular momentum. This conservation is not affected when the interactions are included. For a state with quasi-angular momentum l_z , the OAMs of the two spin states in the lab frame are given by $l_\uparrow = l_z - l$ and $l_\downarrow = l_z + l$, respectively.

Due to the conservation of the quasi-orbital-angular momentum, we can label different phases of the ground state with l_z . The phase diagram of the single-particle Hamiltonian is shown in Fig. 1(c). In the parameter space spanned by δ and Ω_R , three phases with $l_z = 1, 0, -1$ can be identified [14]. The corresponding OAMs in the lab frame are given by $(l_\uparrow, l_\downarrow) = (2, 0), (1, -1), (0, -2)$, respectively. The representative dispersion relation and the spin-dependent density distribution in each phase are also shown in Fig. 1(c). The distinct density distribution makes it very easy to identify each phase experimentally. Note that at fixed finite δ , as Ω_R varies, a phase transition would occur between $l_z = 0$ and $l_z = 1$ (or $l_z = -1$). This is a unique feature due to the quantization of OAM. In a system of SLM coupled atoms, no corresponding phase transition exists: At finite δ , as Ω_R varies, the linear momentum of the atom in the ground state changes continuously without jump.

Four exemplary paths across various phase boundaries, denoted by P_1, P_2, P_3 and P_4 , are shown in Fig. 1(c). Along the paths P_1 and P_2 , the two-photon detuning δ is varied with a fixed Raman coupling strength Ω_R . Along the paths P_3 and P_4 , Ω_R is varied with a fixed δ . We initially prepare the atoms in the spin state $|\downarrow\rangle$ by setting a large two-photon detuning $\delta_i/2\pi\hbar = 400$ kHz. We then switch on the Raman coupling up to the strength Ω_R in 10 ms, subsequently ramp the detuning δ adiabatically to the desired value in 150 ms and hold the system with an additional waiting time of 20 ms for equilibrium. This slow ramp renders the system in the ground state. On the left panel of Fig. 2, we show the spin-resolved density distributions along the four paths. Along path P_1 , we fix $\Omega_R/\hbar\omega = 1604.5$. When δ is large and positive, only the spin state $|\uparrow\rangle$ has a vortex structure in the density distribution, while the spin state $|\downarrow\rangle$ remains in a Gaussian distribution. This region corresponds to the quantum phase $l_z = 1$. We perform an interferometric measurement to detect OAMs of the two spin states $|\uparrow\rangle$ and $|\downarrow\rangle$ [20, 27, 28]. A resonant radio frequency (RF) pulse ($\tau \approx 10\mu\text{s}$) is shined on the atoms before turning on the gradient magnetic field during the TOF, transferring some population from $|\downarrow\rangle$ to $|\uparrow\rangle$. A Gaussian wavepacket and a doubly-charged vortex interfere in the spin state $|\uparrow\rangle$, with the resulting pattern shown on the top of Fig. 2. The measured and the calculated interference patterns are in excellent agreement. These measurements indicate $l_\downarrow = 0$ and $l_\uparrow = 2$. When δ decreases below a threshold, both spin states exhibit vortex structures, indicating that the system has gone across the phase boundary to the quantum phase $l_z = 0$. After applying a resonant

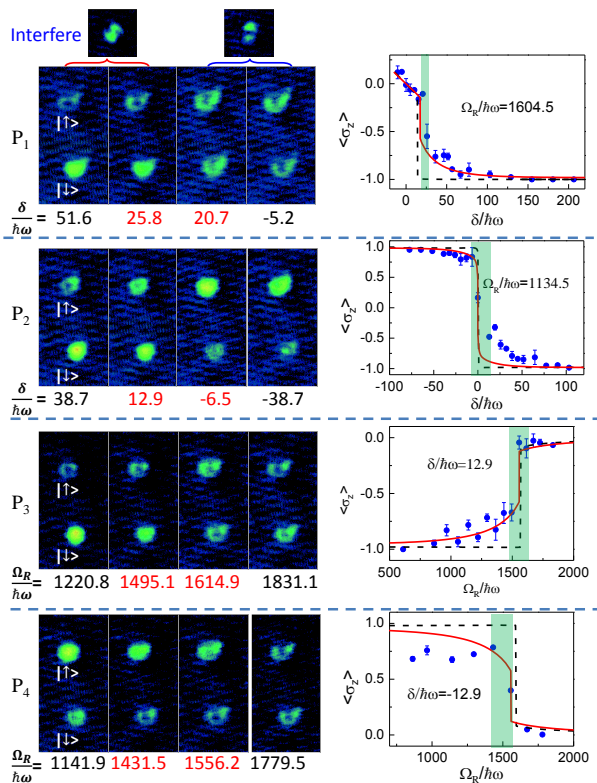


FIG. 2. (color online) Observation of the phase transitions. P_1 , P_2 , P_3 and P_4 denote the four paths indicated in Fig. 1(c). The left panel shows the density distributions of both spin states across the phase boundaries. The right panel shows the corresponding spin polarization $\langle \sigma_z \rangle$. The black dashed (red solid) curves are results from the theoretical calculations for $T = 0$ (finite temperature with $T/T_c = 0.32$, where T_c is the condensate critical temperature in the absence of SOAM coupling). The error bars indicate the standard deviation of experimental measurements. The shaded areas indicate the phase transition regions determined from the left panel. P_1 is for $\Omega_R/\hbar\omega = 1604.5$, P_2 for $\Omega_R/\hbar\omega = 1134.5$, P_3 for $\delta/\hbar\omega = 12.9$ and P_4 for $\delta/\hbar\omega = -12.9$.

RF pulse, the interference pattern indeed confirms that $l_\downarrow = -1$ and $l_\uparrow = 1$ (also shown on the top of Fig. 2). The threshold value for δ at which the density distribution changes character fluctuates statistically when the measurement is repeated over many times. This is reflected in the uncertainty of phase boundary when we plot the phase diagram in Fig 3.

On the right panel of Fig. 2, we plot the spin polarization $\langle \sigma_z \rangle = (N_\uparrow - N_\downarrow)/(N_\uparrow + N_\downarrow)$ along the four paths. Our theoretical calculation for zero temperature indicate that $\langle \sigma_z \rangle \approx \mp 1$ for the phases $l_z = \pm 1$, while $\langle \sigma_z \rangle \approx 0$ for the phase $l_z = 0$. Across the phase boundary, $\langle \sigma_z \rangle$ jumps from one value to another. The finite temperature affects the behaviors of the spin polarization (see Supplemental Material [25]). In our experiment ($T/T_c = 0.32$, T_c is the condensate critical temperature in the absence of the SOAM coupling), the condensate fraction is larger

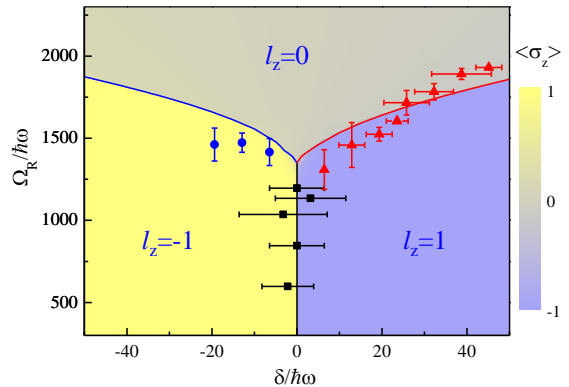


FIG. 3. (Color online) Phase diagram of the SOAM coupled condensate. Three phases are denoted by the quasi-orbital-angular momentum $l_z = 1, 0, -1$, respectively. The solid curves denote the calculated phase boundaries including the many-body interaction. The experimental phase boundaries are determined from measurement shown in Fig. 2. The error bars indicate the experimental uncertainties in determining the boundaries of the phase transitions. The error bars of the red points come from the measurements along the paths P_1 and P_3 , the error bars of the black points from the measurements along the path P_2 , and the error bars of the blue points from the measurements along the path P_4 . The background color denotes the spin polarization $\langle \sigma_z \rangle = (N_\uparrow - N_\downarrow)/(N_\uparrow + N_\downarrow)$.

than 95%. The measured spin polarizations clearly show the jumping behavior across phase boundaries, which are in good agreements with the finite-temperature calculations. The phase transition regions determined by the discontinuous jump of the spin polarization are consistent with those determined by the sudden variation of the spin-resolved density distribution. The discontinuous variation of the spin polarization provides the evidence of the first-order phase transition [15, 16]. Note that here the phase transition versus the variation of the Raman coupling strength is of the first-order. While for the SLM coupling, the phase transition versus the variation of the Raman coupling strength (at zero detuning) is of the second-order.

We use the similar method to observe the phase transitions along the other three paths, and many other similar paths. These measurements allow us to map out the ground-state phase diagram in the parameter space spanned by δ and Ω_R as shown in Fig. 3. Theoretical calculations including the atomic interaction (see Supplemental Material [25]) are also shown as solid curves. The phase diagram of the system is composed of three quantum phases denoted by $l_z = 1, 0, -1$, respectively. Boundaries between these various phases are clearly distinguished both experimentally and theoretically. This phase diagram is very similar to the single-particle phase diagram shown in Fig. 1(c). For ^{87}Rb condensate with

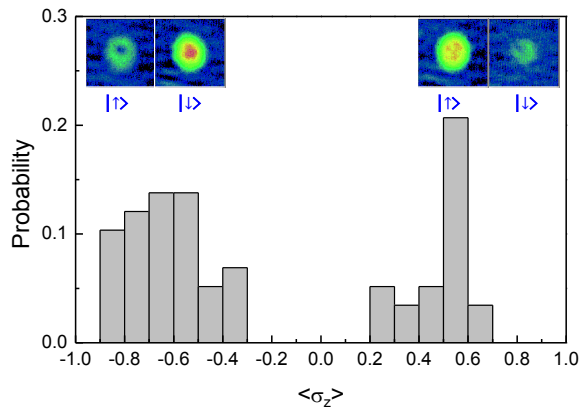


FIG. 4. (Color online) Histogram of the spin polarization $\langle \sigma_z \rangle$ at $\delta = 0$ and $\Omega_R/\hbar\omega = 73.3$. The left (right) insert shows exemplary density distribution for $\langle \sigma_z \rangle < 0$ ($\langle \sigma_z \rangle > 0$). The image size is $600 \mu\text{m} \times 600 \mu\text{m}$.

a relatively weak interaction, our theoretical calculation shows that the interaction only slightly shift the phase boundary.

Nevertheless, the many-body interaction does manifest itself in the following way. On the phase boundary between $l_z = 1$ and $l_z = -1$ (i.e., the black solid curve in Fig. 3), the single-particle ground state has two-fold degeneracy with $l_z = \pm 1$. In the absence of interaction, population can randomly distribute between these two degenerate states without changing the total energy. However, in the presence of the repulsive interaction, in order to minimize the interaction energy, all the atoms should condense into either one of these two states, but not both [15, 16]. In the experiment, we measure the spin polarization $\langle \sigma_z \rangle$ at $\delta = 0$ and $\Omega_R/\hbar\omega = 73.3$, and repeat this measurement 58 times. A histogram of $\langle \sigma_z \rangle$ is presented in Fig. 4, from which we clearly see the distribution of $\langle \sigma_z \rangle$ shows two peaks at $\langle \sigma_z \rangle < 0$ and $\langle \sigma_z \rangle > 0$ [29]. As shown with the inserted images, the vortex structure only exists in the spin state $|\uparrow\rangle$ if $\langle \sigma_z \rangle < 0$ and in the spin state $|\downarrow\rangle$ if $\langle \sigma_z \rangle > 0$. These phenomena indicate that the condensate populates in only one of the two degenerate states with $l_z = \pm 1$, respectively. If both states were randomly populated, the spin polarization would exhibit a flat distribution between -1 and 1. The similar interaction induced state has also been observed in the SLM coupling [30–32]. As a comparison, we measure $\langle \sigma_z \rangle$ for the thermal Bose gas ($T \approx T_c$). In this case, $\langle \sigma_z \rangle$ distributes with one peak at $\langle \sigma_z \rangle \approx 0$ and there is no vortex structure in either spin state (see Supplemental Material [25]).

Due to the quantization of the OAM, all phase transitions in our system are of first-order. It is well known that across first-order phase boundaries, hysteresis loops should show up. In Fig. 5, we display such hysteresis across the boundary between $l_z = 1$ and $l_z = -1$

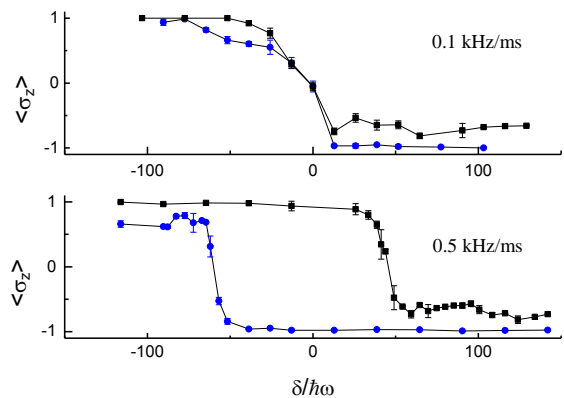


FIG. 5. (Color online) Observation of the hysteresis across the first-order phase transition. We fix $\Omega_R/\hbar\omega = 73.3$ while ramping δ at different rates. The spin polarization $\langle \sigma_z \rangle$ is measured as a function of δ . We initially prepare condensate in the $l_z = 1$ ($l_z = -1$) phase at $\delta/\hbar\omega \approx 142$ ($\delta/\hbar\omega \approx -116$) and then ramp δ across the phase transition as shown with blue circles (black squares). The error bar indicates the standard deviation of experimental measurements. The ramping rates are 0.1 kHz/ms and 0.5 kHz/ms, respectively.

. Here we fix the Raman coupling strength at a small value $\Omega_R/\hbar\omega = 73.3$ while varying δ [33]. The condensate is initially prepared deep in either the $l_z = 1$ or $l_z = -1$ phase. We then ramp δ at different rates and measure the spin polarization $\langle \sigma_z \rangle$. For sufficiently slow ramp as shown in the top panel of Fig. 5, no hysteresis is observed, which indicates that the system have sufficient time to relax into the ground state due to dissipation. By contrast, for fast ramp as shown in the bottom panel of Fig. 5, a clear hysteresis loop is present. This measurement also indicates that, if the ramping rate is slow enough or the waiting time is long enough, we can prepare the condensate in the ground state across the first-order phase transition. Slow ramping process has been used to prepare the ground state across the first-order phase transition before [34–36].

In summary, we report the first experimental observation of the ground-state phase diagram of an SOAM coupled condensate, and demonstrate the first-order phase transitions by probing the spin polarization and the vorticity of the atomic wave function across the phase boundaries. The atoms condense into one of the two degenerate states due to the many-body interaction. The phase transitions at finite δ arise from the quantization of the OAM, and are not present in condensates with SLM coupling. SOAM coupled condensates can be used to probe topological quantum states such as half-skyrmion, vortex-antivortex pairs, Mermin-Ho vortex, and meron pairs [18]. Richer quantum phases exist in the SOAM coupled BEC with higher order LG beams [15]. SOAM coupling can also be extended to systems with higher spins [17] and Fermi gases. It is predicted that there

could exist a stripe phase in the ground-state phase diagram, which represents roughly a superposition of states with different quasi orbital angular momenta [14–17]. Our current work represents a pioneering study towards the use of SOAM coupled quantum gases to explore exotic quantum phases.

We acknowledge fruitful discussions with Hui Zhai, Hui Hu, Xia-Ji Liu, and Chunlei Qu. We also thank Hui Zhai for a critical reading of the manuscript. This work has been supported by the NKRD (National Key Research and Development Program) under Grant No. 2016YFA0301503, NSFC (Grant No. 11474315, 11674358, 11434015, 11747059) and CAS under Grant No. YJKYYQ20170025. HP acknowledges support from the US NSF and the Welch Foundation (Grant No. C-1669). D.Z, T.G. and P.Z. contributed equally to this work.

* pengshiguo@wipm.ac.cn

† kjjiang@wipm.ac.cn

- [1] R. C. Devlin, A. Ambrosio, N. A. Rubin, J. P. B. Mueller, and F. Capasso, *Science* **358**, 896 (2017), and its references.
- [2] M. Z. Hasan and C. L. Kane, *Rev. Mod. Phys.* **82**, 3045 (2010).
- [3] X.-L. Qi and S.-C. Zhang, *Rev. Mod. Phys.* **83**, 1057 (2011).
- [4] Y.-J. Lin, K. Jimenez-Garcia, and I. B. Spielman, *Nature* **471**, 83 (2011).
- [5] P. Wang, Z.-Q. Yu, Z. Fu, J. Miao, L. Huang, S. Chai, H. Zhai, and J. Zhang, *Phys. Rev. Lett.* **109**, 095301 (2012).
- [6] L. W. Cheuk, A. T. Sommer, Z. Hadzibabic, T. Yefsah, W. S. Bakr, and M. W. Zwierlein, *Phys. Rev. Lett.* **109**, 095302 (2012).
- [7] J. Dalibard, F. Gerbier, G. Juzeliūnas, and P. Öhberg, *Rev. Mod. Phys.* **83**, 1523 (2011).
- [8] V. Galitski and I. B. Spielman, *Nature* **494**, 49 (2013).
- [9] H. Zhai, *Rep. Prog. Phys.* **78**, 026001 (2015).
- [10] Z. Wu, L. Zhang, W. Sun, X.-T. Xu, B.-Z. Wang, S.-C. Ji, Y. Deng, S. Chen, X.-J. Liu, and J.-W. Pan, *Science* **354**, 83 (2016).
- [11] M. A. Khomehchi, K. Hossain, M. E. Mossman, Y. Zhang, T. Busch, M. M. Forbes, and P. Engels, *Phys. Rev. Lett.* **118**, 155301 (2017).
- [12] J.-R. Li, J. Lee, W. Huang, S. Burchesky, B. Shteynas, F. C. Top, A. O. Jamison, and W. Ketterle, *Nature (London)* **543**, 91 (2017).
- [13] L. Allen, S. M. Barnett, and M. J. Padgett, *Optical Angular Momentum* (Institute of Physics Publishing, Bristol, 2003).
- [14] M. DeMarco and H. Pu, *Phys. Rev. A* **91**, 033630 (2015).
- [15] K. Sun, C. Qu, and C. Zhang, *Phys. Rev. A* **91**, 063627 (2015).
- [16] C. Qu, K. Sun, and C. Zhang, *Phys. Rev. A* **91**, 053630 (2015).
- [17] L. Chen, H. Pu, and Y. Zhang, *Phys. Rev. A* **93**, 013629 (2016).
- [18] Y.-X. Hu, C. Miniatura, and B. Grémaud, *Phys. Rev. A* **92**, 033615 (2015).
- [19] J. Hou, X.-W. Luo, K. Sun, and C. Zhang, *Phys. Rev. A* **96**, 011603 (2017).
- [20] K. C. Wright, L. S. Leslie, A. Hansen, and N. P. Bigelow, *Phys. Rev. Lett.* **102**, 030405 (2009).
- [21] L. S. Leslie, A. Hansen, K. C. Wright, B. M. Deutsch, and N. P. Bigelow, *Phys. Rev. Lett.* **103**, 250401 (2009).
- [22] H.-R. Chen, K.-Y. Lin, P.-K. Chen, N.-C. Chiu, J.-B. Wang, C.-A. Chen, P.-P. Huang, S.-K. Yip, Y. Kawaguchi, and Y.-J. Lin, *Phys. Rev. Lett.* **121**, 113204 (2018).
- [23] P.-K. Chen, L.-R. Liu, M.-J. Tsai, N.-C. Chiu, Y. Kawaguchi, S.-K. Yip, M.-S. Chang, and Y.-J. Lin, *Phys. Rev. Lett.* **121**, 250401 (2018).
- [24] T. Gao, J.-S. Pan, D. Zhang, L. Kong, R. Li, X. Shen, X. Chen, S.-G. Peng, M. Zhan, W. V. Liu, et al., arXiv: 1805.04727 (2018).
- [25] See Supplemental Material for the experimental procedure, measurement of the spin polarization for the thermal gas, and theoretical calculations of the phase boundaries and spin polarizations.
- [26] F. Schmidt, D. Mayer, M. Hohmann, T. Lausch, F. Kindermann, and A. Widera, *Phys. Rev. A* **93**, 022507 (2016).
- [27] M. R. Matthews, B. P. Anderson, P. C. Haljan, D. S. Hall, C. E. Wieman, and E. A. Cornell, *Phys. Rev. Lett.* **83**, 2498 (1999).
- [28] M. F. Andersen, C. Ryu, P. Cladé, V. Natarajan, A. Vaziri, K. Helmerson, and W. D. Phillips, *Phys. Rev. Lett.* **97**, 170406 (2006).
- [29] In the measurements, the average value of the spin polarizations $\overline{\langle\sigma_z\rangle}$ is about -0.63 (0.55) at $\langle\sigma_z\rangle < 0$ ($\langle\sigma_z\rangle > 0$). Due to the finite temperature, the absolute value of the spin polarization $|\langle\sigma_z\rangle|$ at $\delta = 0$ can be smaller than 1, as shown with the theoretical calculation in Fig.2.
- [30] T.-L. Ho and S. Zhang, *Phys. Rev. Lett.* **107**, 150403 (2011).
- [31] Y. Li, L. P. Pitaevskii, and S. Stringari, *Phys. Rev. Lett.* **108**, 225301 (2012).
- [32] S.-C. Ji, J.-Y. Zhang, L. Zhang, Z.-D. Du, W. Zheng, Y.-J. Deng, H. Zhai, S. Chen, and J.-W. Pan, *Nature Phys.* **10**, 314 (2014).
- [33] We find that the potential barrier between the two degenerate states is high at a small Raman coupling strength, which makes the area of the hysteresis loop big. The similar effect has also been demonstrated in ref. [34].
- [34] A. Trenkwalder, G. Spagnolli, G. Semeghini, S. Coop, M. Landini, P. Castilho, L. Pezzé, G. Modugno, M. Inguscio, A. Smerzi, et al., *Nature Phys.* **12**, 826 (2016).
- [35] C. Hammer, C. Qu, Y. Zhang, J. Chang, M. Gong, C. Zhang, and P. Engels, *Nat. Commun.* **5**, 4023 (2014).
- [36] Z. Fu, P. Wang, S. Chai, L. Huang, and J. Zhang, *Phys. Rev. A* **84**, 043609 (2011).